Micromachining in Plastics Using X-Ray Lithography for the Fabrication of Micro-Electrophoresis Devices

S. M. Ford

J. Davies

B. Kar

S. D. Qi

S. McWhorter

S. A. Soper[1]

Department of Chemistry,
Louisiana State University,
Baton Rouge, LA 70803-1804

C. K. Malek
Center for Advanced Microstructure
and Devices,
Louisiana State University,
Baton Rouge, LA 70810

Micromachining was performed in polymethylmethacrylate (PMMA) using X-ray lithography for the fabrication of miniaturized devices (microchips) for potential applications in chemical and genetic analyses. The devices were fabricated using two different techniques: transfer mask technology and a Kapton® mask. For both processes, the channel topography was transferred (1:1) to the appropriate substrate via the use of an optical mask. In the case of the transfer mask technique, the PMMA substrate was coated with a positive photoresist and a thin Au/Cr plating base. Following UV exposure, the resist was developed and a thick overlayer (~3 μm) of Au electroplated onto the PMMA substrate only where the resist was removed, which acted as an absorber of the X-rays. In the other technique, a Kapton® film was used as the X-ray mask. In this case, the Kapton® film was UV exposed using the optical mask to define the channel topography and following development of the resist, a thick Au overlayer (8 μm) was electrodeposited onto the Kapton® sheet. The PMMA wafer during X-ray exposure was situated directly underneath the Kapton® mask. In both cases, the PMMA wafer was exposed to soft X-rays and developed to remove the exposed PMMA. The resulting channels were found to be 20 μm in width (determined by optical mask) with channel depths of ~50 μm (determined by x-ray exposure time). In order to demonstrate the utility of this micromachining process, several components were fabricated in PMMA including capillary/chip connectors, injectors for fixed-volume sample introduction, separation channels for electrophoresis and integrated fiber optic fluorescence detectors. These components could be integrated into a single device to assemble a system appropriate for the rapid analysis of various targets.

Introduction

In most analytical assays, the process involves a separation step to sort the individual molecules through molecular properties, such as size and/or charge. Significant research efforts have recently been invested into developing new separation methods, which offer increased separation efficiencies and reduced development times. One such separation platform is capillary electrophoresis (CE), which has been demonstrated to be an important tool in many analyses due primarily to the ability to generate high plate numbers, the speed of the technique, and its relative simplicity. In this format, a capillary tube made of fused silica with a diameter of 50–100 μm and a length of 30–50 cm is filled with an appropriate matrix and a high electric field applied across the tube. CE has been particularly useful for the analysis of both single and double-stranded DNAs [1–4]. In the CE separation of restriction fragments (dsDNAs) using a free-flowing entangled polymer as the sieving matrix, it is not atypical to see complete separations developed in as little as 10–20 minutes under appropriate operating conditions [5–10]. However, unlike the CE analysis of analytes such as amino acids or other small molecules, the separation of DNAs requires special considerations, such as wall coatings to minimize the electro-osmotic flow (EOF) [11], and a fractionating medium, since the oligonucleotides effectively migrate at the same rate in free solution when the base numbers in the oligonucleotides exceeds 20 [12].

An attractive alternative to conventional CE is micro-electrophoresis, which basically consists of microchannels (10–50 μm) etched into an appropriate substrate material [13–24]. These devices are typically prepared in glass using photolithographic procedures. The channel fabrication involves coating the glass substrate with a suitable photoresist, placement of a photomask on the substrate, UV exposure, development of the exposed resist, etching using a buffered HF solution (wet chemical etching), and enclosure of the channels by heat annealing a glass coverslip to the substrate. The motivation for using glass stems from the fact that it exhibits excellent optical properties allowing ultrasensitive fluorescence detection and, in addition, the surface structure is similar to conventional capillary tubes producing comparable EOFs and immobilization chemistries. Using these devices, researchers have demonstrated the ability to separate analytes, such as DNA restriction fragments, with high resolution in as little as 20–40 s with column lengths of 3–5 cm [25, 26]. Another attractive feature associated with these devices is the ability to incorporate various sample preparation steps onto the microchip itself, minimizing sample handling and resulting in the ability to analyze ultrasmall volumes of materials and consume minimal amounts of reagents [19, 27–30].

One of the difficulties associated with the fabrication of these devices is the etching process used to produce the microchannels. It is difficult to produce narrow channels with reasonable depths due to the isotropic nature of the etching, resulting in severe mask undercutting. Indeed, it has been reported that the

[1] Corresponding author.

Contributed by the Bioengineering Division for publication in the JOURNAL OF BIOMECHANICAL ENGINEERING. Manuscript received by the Bioengineering Division June 14, 1998; revised manuscript received October 1, 1998. Associate Technical Editor: M. Toner.

aspect ratio in wet-etching for micro-electrophoresis systems has been estimated to be 1:1 (defined as the amount of undercutting to the vertical etch depth) [28]. As a result, it will be difficult to produce channels using these techniques that can accommodate certain insert devices, such as fiber optics and capillary tubes for interconnecting devices, which demand narrow channels with reasonably deep depths.

An alternative to wet-etching in glass to produce micro-devices is X-ray lithography [31]. In this technique, X-ray sensitive resists are exposed to soft X-rays resulting in polymer degradation, which can subsequently be developed and produce channels with extremely high aspect ratios [31]. One of the common X-ray sensitive resists that is used in X-ray etching is polymethylmethacrylate (PMMA, Plexiglas). PMMA has been micromachined to produce such structures as gears, micro-optics, and other three-dimensional structures [32].

Some of the properties associated with PMMA that can potentially make it an ideal material for performing electrophoretic-based assays include: (1) Its dielectric strength is significantly better than that of glass (450–500 V/mil for PMMA; 300 V/mil for fused silica). This should allow the ability to produce devices with high packing densities of electrophoretic separation channels and the application of high electric fields with no material breakdown effects. (2) PMMA possesses a thermal conductivity similar to glass and/or fused silica (0.6×10^{-3} cal/cm^2/s for PMMA; 3×10^{-3} cal/cm^2/s for fused silica). This will allow the application of high electric fields with efficient dissipation of Joule heat (resistive heating of carrier buffer due to current flow giving rise to convective mixing of sample zone) generated in the separation channel preserving system performance. (3) The surface of PMMA does not contain a pH ionizable functional group as does glass or fused silica arising from deprotonation of the silanol groups. As such, PMMA is expected to display a significantly smaller EOF, especially at high pH values. Therefore, in cases where the EOF is detrimental to the electrophoretic separation, for example in DNA separations, polymer coating of the wall is not required. The difficulty associated with these wall coatings is that they can degrade under extended high electric field operation, which can limit the effective operational lifetime of the microdevice. Recently, an acrylic-based micro-electrophoresis device constructed using injection molding techniques was presented, which showed the high resolution separation of DNA restriction fragments in channels that were not polymer-coated [33]. In addition, work has demonstrated the ability to use PDMS-based micro-electrophoresis devices to fractionate dsDNAs in channels that were not coated with a polymer layer as well [34]. Also, work has appeared that utilized PMMA as the substrate for micro-electrophoresis with the channels machined into the device using imprinting techniques [35]. However, in these cases, the aspect ratios produced following micromachining were not significantly better than those obtained using wet etching in glass.

Figure 1 shows the processing steps required for the fabrication of a Kapton® and transfer mask appropriate for X-ray micromachining. For both mask technologies, one can iteratively alter the device topography or channel dimensions without investing a significant amount of financial resources into a permanent X-ray mask [36, 37]. After the optical mask has been prepared, which defines the channel dimensions and the device topography, it is aligned onto a PMMA or Kapton® film substrate, which has a thin Au/Cr plating base and a positive (or negative) photoresist deposited onto it. Once the mask is situated, the assembly is exposed to UV light, resulting in a 1:1 transfer of the mask pattern to the photoresist. This is followed by development of the exposed resist and addition, via electroplating, of a thick layer of Au to act as the X-ray absorber during exposure. After development of the unexposed resist, the PMMA is either placed directly in the X-ray beam (transfer mask) or situated directly behind the Kapton® film and placed in the X-ray beam, exposed for the prescribed amount of time, and subsequently developed in a solvent to remove degraded polymer. Finally, a cover plate is bonded to the substrate to enclose the channels. Basically, the channel depth is controlled by the exposure time of the PMMA to the X-ray beam with the added benefit that very little undercutting results.

While PMMA does possess some advantages for electrophoresis, one potential difficulty is that it does not display optical properties comparable to fused silica or glass. For example, PMMA can produce autofluorescence, especially when excited with a laser in the UV region of the electromagnetic spectrum. This can produce high backgrounds, degrading the signal-to-noise ratio (SNR) in ultrasensitive fluorescence measurements. In addition, imperfections in the PMMA (areas of inhomogeneous refractive index produced by mechanical stress during fabrication) can cause complex refraction patterns, degrading the imaging quality of the optical system.

In this paper, we wish to present results on the fabrication and operational characteristics of miniaturized devices constructed in PMMA using X-ray lithography with various functional components for the potential use in analyses requiring an electrophoresis separation step. The devices consisted of connectors for interfacing conventional capillary tubes to microchips for sample introduction, a fixed volume injector, a serpentine column of 6 cm total length to produce sufficient plate numbers for high-demanding separations and a fiber-optic fluorescence detector. This detector was composed of a solid-state near-IR laser and avalanche photodiode. In addition, two different techniques for mask preparation will be discussed for high aspect ratio micromachining, transfer mask, and Kapton® mask methods.

Experimental Section

X-Ray Micromachining in PMMA. The micromachining in PMMA using the transfer mask technique followed procedures previously outlined by Vladimirsky and co-workers [36, 37]. The process involved the construction of an optical mask followed by transferring the mask topography to an X-ray sensitive resist coated with a positive UV photoresist. After exposure to UV light and subsequent development, a thick layer of X-ray absorber was applied to the exposed areas to produce the X-ray mask, which, after exposure, was removed from the substrate. The topography of the micro-electrophoresis device is shown in Fig. 2. It consisted of an injection cross with the ability to electroinject sample volumes of 100 pL, a separation column with a serpentine type geometry [16], and two channels 50 μm in width to allow insertion of optical fibers to deliver laser light and collect emission for fluorescence detection without the need of this light traversing the PMMA substrate, which could generate high backgrounds. The fiber channels were situated at a 50 deg angle with respect to each other in order to reduce excitation light from being collected by the emission fiber. All other channel widths were set to 20 μm with channel depths, determined primarily by the exposure time to the X-rays, of 50 μm. In order to aid in the bonding of the PMMA cover to the PMMA microdevice, the channel walls were 100 μm thick.

Optical Mask Preparation. A schematic of the steps used for fabrication of the optical mask is shown in Fig. 3. A microposit 1400-23 positive photoresist (Microchem Corp., Newton, NJ) was spin coated onto a quartz plate with chromium at 2700 rpm for a period of 30 s, resulting in a thickness of approximately 0.5 μm. The quartz plate was placed on a pattern generator (RTS) and the pattern transferred directly to the resist. Once the pattern was transferred, the resist was developed for 30 s in 454 Developer (Microchem Corp.). The plate was then rinsed with copious amounts of distilled water and placed in a Cr etch bath. The mask was etched for a total of 5 minutes in 30 s

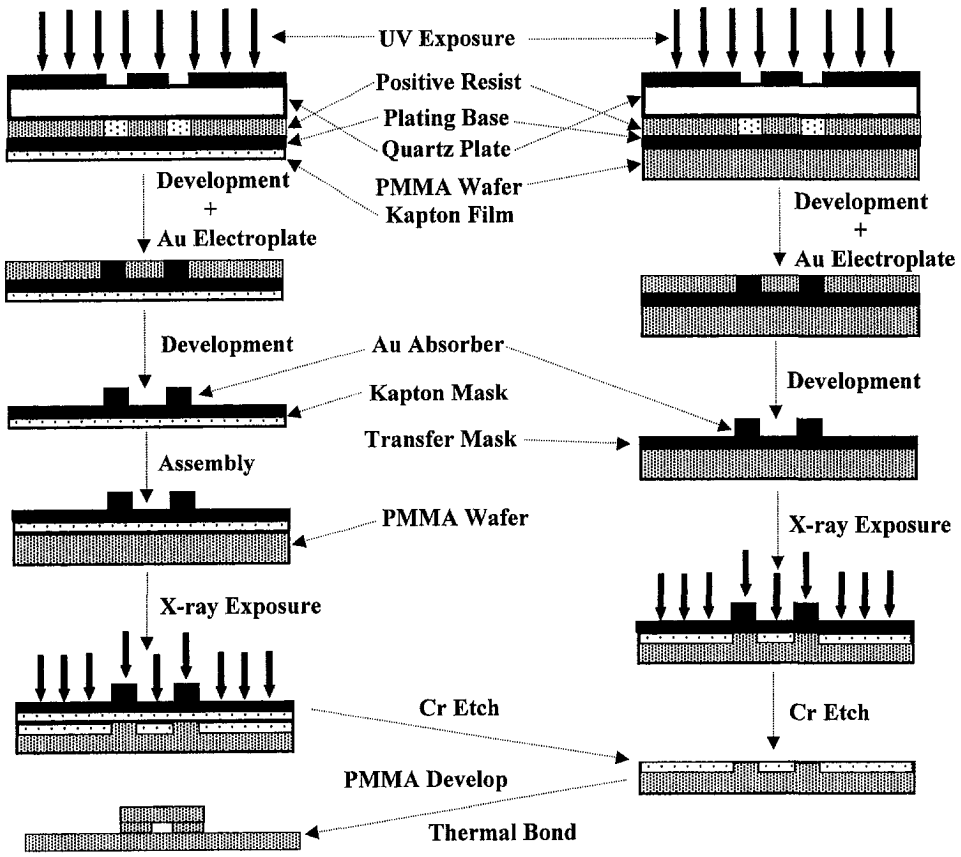

Fig. 1 X-ray lithography processing steps using transfer mask and Kapton® film technologies

intervals with water rinsing and drying between each submersion. In the final step, a 90 s etch was performed.

Transferring Pattern to PMMA Substrate. The PMMA substrates were cut into 4 in. circular wafers with alignment crosses and holes. After cutting, the wafers were cleaned with isopropyl alcohol and then thoroughly rinsed with water. After the water rinsing, the wafers were baked at 80°C for 25–30 minutes and exposed to UV light for 30 s. The dried wafer was placed into a thermal evaporator (Temescal, Fairfield, CA) and a 5 nm coating of Cr followed by the deposition of a 100 nm layer of Au, which served as the plating base. Microposit 1400-23 (positive resist) was then spin coated onto the Au/Cr plated wafers at 1000 rpm for 30 s (resist thickness = 1.0 μm) and baked for 30 minutes at 100°C. The PMMA wafer was then aligned onto the optical mask using alignment holes cut into the PMMA and placed on a UV exposure station (Oriel, Stratford, CT) and exposed for 20 s. The wafer was then developed (30 s) and rinsed with distilled water followed by air drying. After resist development, electrical contacts were made to the wafer and it was placed in a gold solution (Sel Rex BDT 510 electroplating gold solution, Enthone-OMI). The solution was stirred while a constant current of 10 mA was applied. The wafer remained in the bath for 30 min, resulting in a gold thickness of about 3 μm.

Kapton® Mask Preparation. Fabrication of the Kapton® mask followed procedures previously described [38]. Briefly, the Kapton® mask consisted of a thin sheet of Kapton®, which was relatively transparent to X-rays and served as a support for the X-ray mask defining the device topography. In this case, the mask consisted of a thick Au layer to act as the X-ray absorber. To the thin sheet of Kapton®, a 50 Å layer of Cr was deposited thermally followed by the deposition of 100 nm of Au, which served as the plating base. A Shipley AZ 4620 positive photoresist (Clariant, Somerville, NJ) was spin coated onto the Kapton® film at a speed of 1500 rpm for 30 s. In this case, a thicker layer of resist was deposited onto the Kapton® film in order to allow a thicker layer of Au overlayer, since the mask was intended to be used repeatedly. Following resist spin coating, the Kapton® film was baked at 95°C for 30 min and slowly cooled to room temperature. The resist was then exposed to UV light for 30 s with the optical mask placed directly on top of the Kapton® film. The exposed resist was then developed with an AZ 400K positive resist developer (Shipley). After resist development, a thick layer of Au (8 μm) was applied to the Kapton® film via electroplating at a current density of 2 mA/cm^2 with the final step consisting of removing the undeveloped positive resist.

X-Ray Exposure and Development. The wafers were exposed with 7–9 Å synchrotron radiation at our Center for Advanced Microstructure and Devices (CAMD) facility. The exposure time varied, depending upon the stored current inside the synchrotron ring and the desired dosage, typically 4,000 mJ/cm^2. For the transfer mask method, the entire PMMA wafer with Au overlayer was inserted into the X-ray beam. In the case of the Kapton® mask, a blank PMMA wafer was placed directly adjacent to the Kapton® film and inserted into the X-ray beam. After X-ray exposure, the wafers were developed in GG developer (15 percent water, 60 percent butoxyethanol, 20 percent terahydrooxazine, 5 percent aminoethanol) at 36°C for 20 min with sonication and then rinsed in GG rinse at 36°C. Following development, the Au/Cr layer was removed by simply pealing the Au layer from the PMMA substrate and removing residual Cr using a Cr etching solution (for transfer mask case only). Harsh acid removal steps to eliminate the Au/Cr layer were avoided to prevent hydrolysis of the methyl ester groups of the PMMA, producing a surface-bound weak acid in the micro-

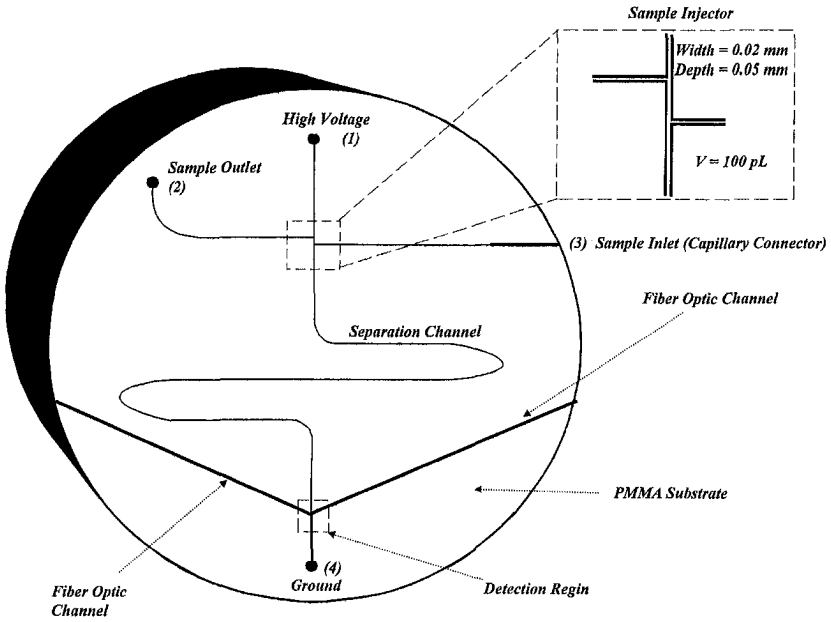

Fig. 2 Topography of the micro-electrophoresis device. The integrated device consists of capillary connector to allow simple sample introduction (sample inlet) or interconnection to other devices, fixed-volume sample injector (see inset), separation channel of 6 cm total length, and a dual fiber-optic fluorescence detector.

machined channel, which would result in significant EOFs. The channels were characterized using both step-scan profilometry and scanning electron microscopy (SEM).

Bonding of PMMA Cover. In order to enclose the micromachined channels to allow fluid flow through the device, we developed a bonding procedure to seal a top plate to the PMMA substrate. The top plate was also made from PMMA (9 × 4 cm) and was cut to a size to completely enclose all of the electrophoresis channels. Prior to bonding, access holes were drilled into the top plate to accommodate pipet tips, which served as buffer and waste reservoirs. Both the bottom and cover plates contained alignment holes that fit into a jig to align the two plates prior to sealing. The thermal bonding process involved heating both the top plate and substrate on a hot plate to temperatures of 150°C, slightly above the glass transition temperature (T_g) for PMMA, for 5–10 minutes. Heating only the surfaces of the PMMA prevented outgassing and bubble inclusion, which occurred when the entire PMMA blocks were heated in a furnace. After the prescribed heating period, the substrate was then immediately placed in the alignment jig and the bottom plate inserted. Following this, a 50 lb copper weight was placed on the PMMA sheets and the entire assembly allowed to cool slowly to room temperature in a programmable oven over an approximate 2 h period of time. The integrity of the bonding process was confirmed using an optical microscope for visual inspection.

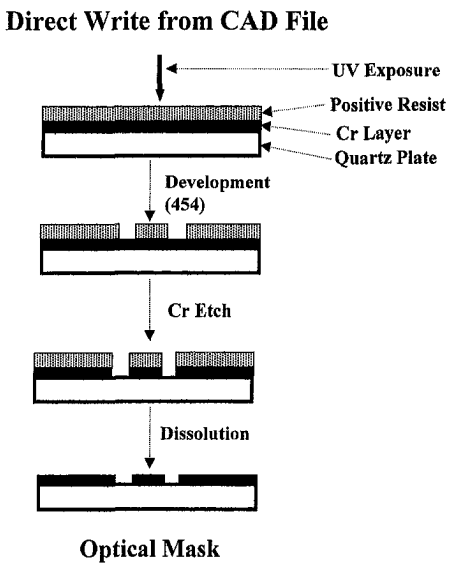

Fig. 3 Schematic showing the processing steps for fabrication of the optical mask. See text for description of processing steps.

Near-IR Laser-Induced Fluorescence Detector. A block diagram of the laser-induced fluorescence detector is shown in Fig. 4. The excitation source consisted of a GaAlAs diode laser with a principal lasing line of 750 nm at room temperature, which produced 5 mW of average power (Melles Griot, Irvine, CA). The laser contained external cavity optics to produce a circular beam that was pseudo-Gaussian and was temperature stabilized with an on-chip thermoelectric cooler. The laser beam was launched into a single mode fiber (core diameter = 8 μm; cladding diameter = 125 μm), which was placed in a fiber coupler (Melles Griot). In order to allow insertion of the fiber into the 50 × 50 μm channel, the terminal end was etched in buffered HF and visually inspected under a microscope until the diameter of the fiber was slightly below 50 μm. The emission was collected by another single mode fiber and collimated using a second fiber coupler. The collimated emission was spatially filtered and then further isolated from the scattering and excitation photons using an eight-cavity bandpass filter with a center wavelength of 780 nm and a half bandwidth of 20 nm (Omega Optical, Brattleboro, VT). The fluorescence was then focused onto the photoactive area of the detector using a 20× microscope objective. The detector was a single photon avalanche photodiode (SPAD), which was operated in a Geiger mode and actively quenched to permit processing of high count rates without saturating the detector (EG&G Electrooptics, Vaudreuil, Canada). The data were fed into a counting board with the data processed and displayed on a PC with data acquisition

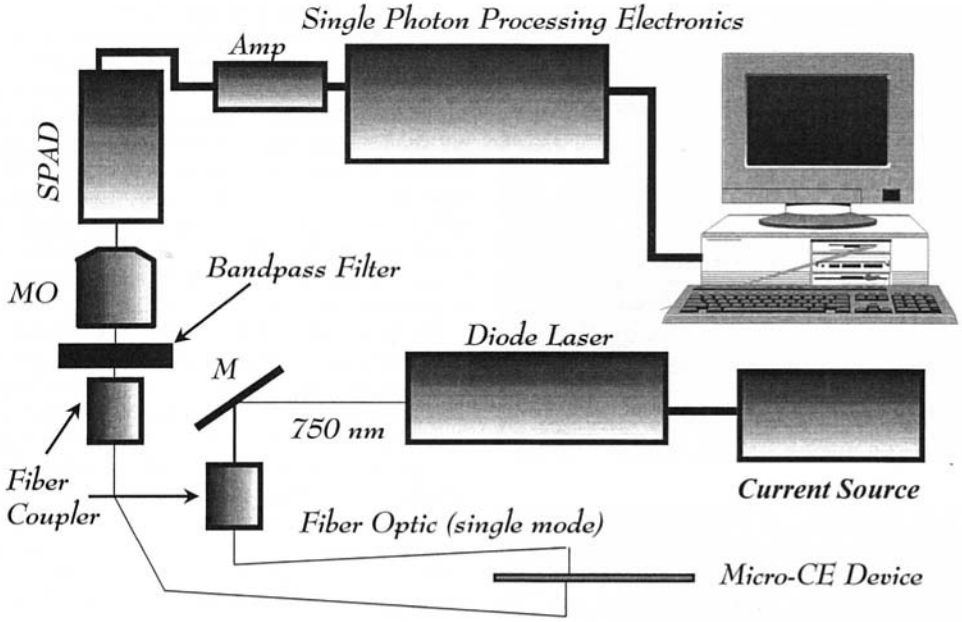

Fig. 4 Near-infrared, laser-induced fluorescence system for on-chip fluorescence detection. The laser source was a GaAlAs diode laser with a principal lasing line of 750 nm (25°C) with 10 mW of output power. The laser was focused onto one face of a single-mode optical fiber using a fiber coupler with the opposite end of this fiber sealed into the microdevice. The emission was collected by another single mode optical fiber, collimated with another fiber coupler, and focused onto the face of a single photon avalanche diode using a microscope objective (MO) for transduction. The output of the single photon avalanche diode (SPAD) was amplified 20× (Amp) with the pulses processed using a counting board interfaced to a PC computer.

software written in LabView (National Instruments, San Antonio, TX).

Reagents. The near-IR dye, NN382, used for system evaluation was obtained from Li-COR (Lincoln, NE) and was dissolved in DMF and stored in the dark in a freezer until used. For electro-osmotic measurements, the appropriate amount of buffering salt (sodium phosphate) was added to ultrapure water and brought to the required pH using either HCl or NaOH. After pH adjustment, polystyrene beads (id = 0.8 μm, Duke Scientific) were added to the buffer. The EOF was measured by observing the rate of movement of these neutral beads through the micromachined channels using an optical microscope (Optiphot II, Nikon).

Electrophoresis of Near-IR Dye. For the free solution micro-electrophoresis, reservoirs 1, 2, and 4 (see Fig. 2) were filled with the running buffer and reservoir 3 (microvial external to chip) filled with the dye solution. Sample injection was performed by applying −500 V to reservoir 3 and grounding reservoir 2. After the desired amount of time, the applied voltage was switched to reservoir 1 (−1800 V) and reservoir 4 was grounded. The running buffer used in these experiments consisted of a 20 mM solution of borate (pH = 9.2). The dye solution was diluted in the running buffer at the appropriate concentration.

Results and Discussion

One of the principle advantages of machining in PMMA using soft X-rays is that one can fabricate devices with narrow and deep channels (i.e., high aspect ratio) due to the fact that isotropic etching is not used. Figures 5 and 6 show SEMs of several functional components machined into the PMMA substrate using the transfer mask technique. As can be seen, the channel geometry was well defined with excellent contrast. From high-resolution SEM micrographs of the micromachined channels and that of the optical mask, the amount of undercutting was estimated to be ~10 nm. Profilometer traces indicated that the channel depth in this particular case was 40 μm. Based upon these values, the aspect ratio was determined to be 1:4000, considerably better than the value of 1:1 measured for wet-chemical etching of glass [28]. It should be pointed out that one could potentially obtain improved aspect ratios by increasing the exposure time in the X-ray beam due to the minimal amount of undercutting that results during X-ray etching of the resist (PMMA). It can also be seen from Figs. 5 and 6 that the walls and floor of the device are very smooth. In this case, the smoothness of the floor of the device is determined by the constant flux of X-ray photons across the exposed area. The smoothness of the wall was primarily determined by the quality of the optical mask. It was also important to investigate the integrity of the microfabricated channels after thermal bonding. From an optical microscopic investigation of the channels after thermal boding (data not shown), it was found that no bowing or deformation of the micromachined channels were observed using our thermal bonding process.

Using the transfer mask technique, several difficulties were encountered, namely the long processing time that was required to fabricate devices. For each device, an electroplating step was necessary, as well as UV exposure and photoresist development. In addition, we found that many times, particulates were discovered on the device during electroplating, producing void volumes (unswept volumes) that reduced device performance or made the device nonfunctional (excessive device failure rate).

In order to reduce device fabrication time and failure rate, a Kapton® mask procedure was investigated. In this method, the device topography was transferred to the Kapton® polymer and a thick Au layer (absorber) electroplated onto the Kapton® film. Once the Kapton® mask was prepared, one only needed to position a blank PMMA wafer directly behind the mask and X-ray expose the substrate. In addition, this mask can be used for multiple X-ray exposures. In all cases, the wafers exposed using the Kapton® mask produced similar results in terms of device aspect ratios compared to the transfer mask method (data not shown). However, since the Kapton® does absorb some of

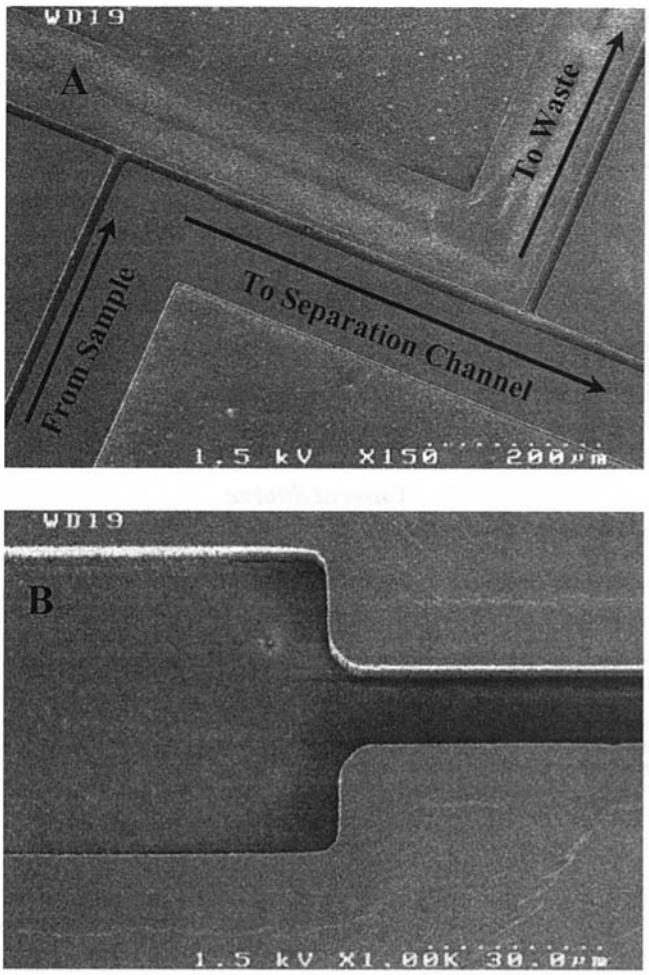

Fig. 5 Scanning electron micrographs of the processed PMMA substrate following X-ray exposure and development. The components depicted in this figure are the fixed volume injector (A) and the capillary connector (B). In (A), the channels are 20 μm in width and approximately 50 μm in depth. In (B), the channel is ~55 μm in width and 50 μm in depth to allow insertion of a capillary tube. The micromachined channel is tapered to 20 μm to accommodate a capillary tube with a 20 μm internal diameter.

the X-rays, longer exposure times were required to reach the desired channel depths (8–12 h). An advantage associated with the Kapton® mask was also found in terms of device integrity. In the transfer mask technique, the PMMA was directly exposed to the X-ray beam whereas in the case of the Kapton® mask, some of the lower energy X-rays were absorbed by the Kapton® film. In the case of the transfer mask, we noticed in many cases cracking and bubble formation of the exposed PMMA polymer following development. For the devices fabricated using the Kapton® mask, the appearance of these cracks and bubbles were not observed. We attributed this to the Kapton®, which acts as a filter cutting off much of the lower energy X-rays from penetrating the PMMA substrate causing bubble and cracking in the substrate.

We next investigated the magnitude and pH profile of the EOF in these PMMA-based devices. The EOF pH profiles for both fused silica and PMMA (X-ray etched) are shown in Fig. 7(*A*). Fused silica demonstrated the common sigmoidally shaped profile, with a large increase in the EOF at pH ~6, resulting from deprotonation of the surface silanol groups. In the case of PMMA, the EOF was found to be relatively independent of changes in the pH, consistent with its surface structure. At pH = 10.0, the EOF was found to be 1.9×10^{-4} cm^2/Vs for PMMA and 10.2×10^{-4} cm^2/Vs for fused silica, an approximate fivefold difference. In order to determine the effects of X-rays on the surface structure of PMMA, which may affect the magnitude of the EOF, we carried out similar EOF investigations in a channel, which was mechanically etched in the PMMA. The EOF in the mechanically etched channel (data not shown) was similar to the X-ray etched channel. Therefore, the X-rays most likely result in scission of the polymer backbone and not oxidation of the functional groups to carboxylates, which would produce a much larger EOF and show a pH-dependent profile. This is consistent with previous literature which has shown that the use of soft X-rays results primarily in polymer backbone scission [39, 40].

We next compared the ability of our device to dissipate Joule heat when high electric fields are applied and compared it to a conventional fused silica capillary tube of similar dimensions. This experiment was carried out by monitoring the current produced when different voltages were applied to the microdevice or capillary tube. When the current is plotted versus the applied voltage, the resultant plot should be linear, with deviations resulting when the device was unable to effectively dissipate the generated Joule heat. As can be seen from the Ohms' plots shown in Fig. 7(*B*), the microdevice showed deviations from linearity at an applied field strength of 720 V/cm for this high

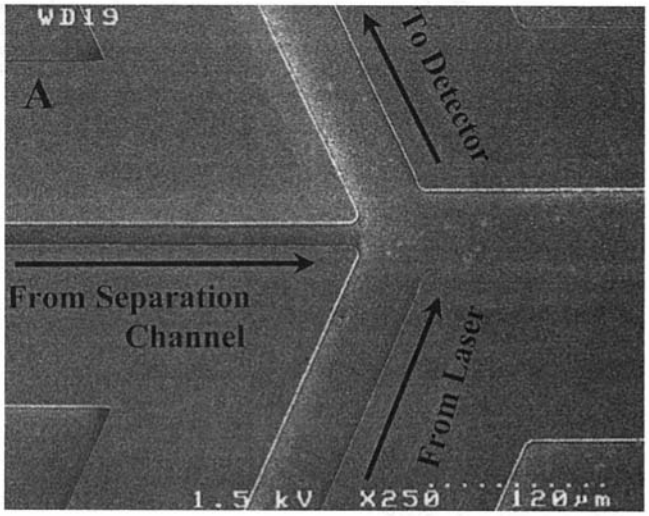

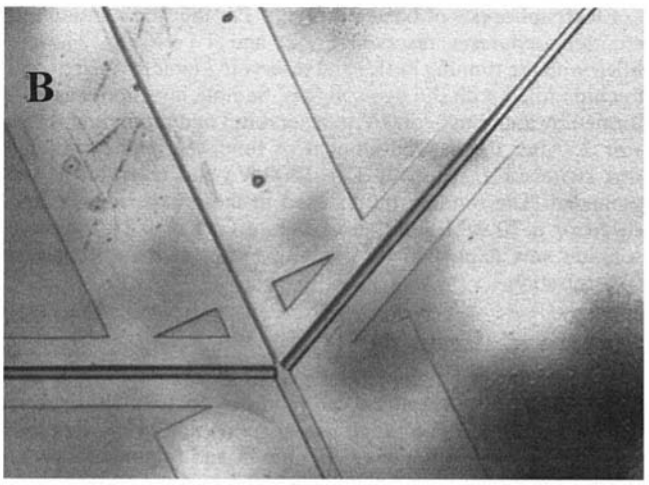

Fig. 6 SEM of the dual fiber optic detector micromachined in PMMA (A). In (B) is shown an optical micrograph of two single-mode fibers inserted into the device. The fibers were etched using HF to a diameter of approximately 45 μm and then inserted into the micromachined channels using a three-axis microtranslational stage. The process was monitored under an optical microscope.

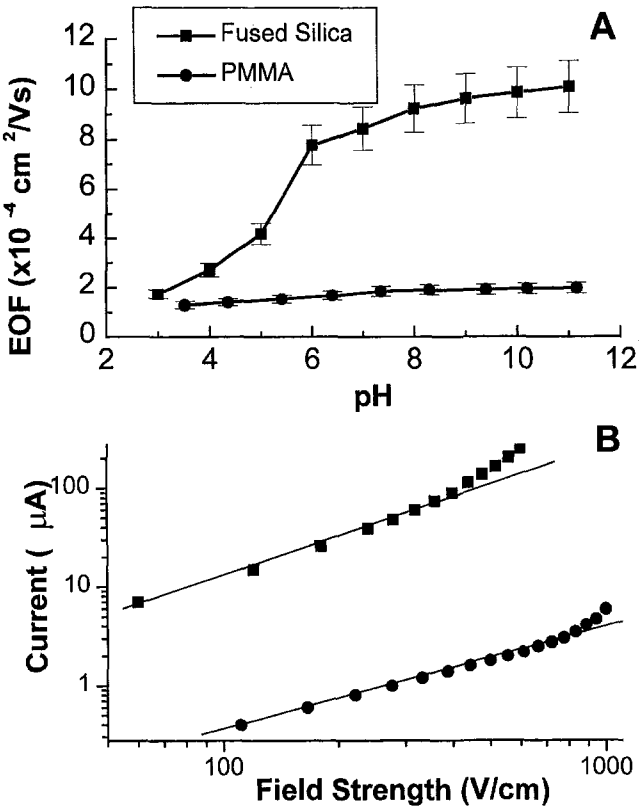

Fig. 7 Electro-osmotic flow profiles for PMMA and fused silica taken as a function of the buffer pH (A). The EOFs were measured by monitoring the linear velocity of small microbeads (0.8 μm i.d.) under an optical microscope with an applied electric field and the appropriate buffer solution. The linear velocities were converted into electro-osmotic flows (cm^2/Vs) by dividing the linear velocity by the field strength. The error bars shown represent the precision in the measurement and not variability between devices. (B) Ohm's plot showing the measured current flow in the fused silica (i.d. = 50 μm) and micromachined PMMA channel (50 × 50 μm) as a function of the applied electric field. In this case, the buffer used was 20 mM borate at a pH of 9.2.

conductivity buffer, while the capillary tube produced nonlinearities at a field strength of 420 V/cm.

Free solution electrophoresis was then carried out on the near-IR dye, NN382 with the results shown in Fig. 8. Interestingly, the electrophoresis was run in a reverse mode, with the sample injection end being negative (cathodic) and the detection end positive (anodic). In the case of the fused silica electrophoresis analysis of this dye, normal polarity was required (injection end anodic). This is due to the smaller EOF associated with the PMMA device compared to fused silica. In Fig. 8(A), three different injection times were used in order to fill the fixed volume injector for sample introduction while in Fig. 8(B), three different field strengths were applied to the separation device to investigate system performance. System performance was determined by calculating the theoretical plate numbers (N) for pseudo-Gaussian peaks using the expression

$$N = 5.54\left(\frac{t_{mig}}{w_{1/2}}\right)^2$$

where t_{mig} is the migration time (s) and $w_{1/2}$ is the width of the electrophoretic peak at the half height (s). As can be seen from Fig. 8(A), the dye migrates through this 6.0 cm length channel (injection to detection points) in approximately 300 s at a field strength of 50 V/cm. Also apparent from these data is that the peak area increased as the injection time was increased to 15 s. Further increases in the injection time did not significantly increase the peak area, indicating that the 15 s time period at this field strength was sufficient to fill the fixed volume injector. Calculation of N for these injection times yielded values of 24,226, 41,550, and 38,954 plates/m for injection times of 5, 10, and 15 s, respectively. In order to reduce the migration time, the field strength was then increased and the resultant plate numbers calculated for three different field strengths. From Fig. 8(B), the migration time was reduced to ~44 s when the field strength was increased to 333 V/cm. Plate numbers calculated for this data indicated that the efficiency was similar for all three electric fields (~24,500 plates/m). We note here that the plate numbers are relatively low compared to values typically obtained with micro-electrophoresis devices [28, 41]. We have attributed this reduced performance to interactions between the wall of the device and the hydrophobic dye molecule, which we have shown to occur in conventional capillary tubes when electrophoresing these type of dyes [42]. This interaction would be expected to be more pronounced in the PMMA-based device since the walls are more hydrophobic than a deprotonated fused silica surface. In order to alleviate this loss in performance, small amounts of organic solvents can be added to the run buffer.

The mass detection limit of the detection system was investigated next. Due to the small size of the fiber, it would be expected that the collection efficiency of the system would be low. In the present configuration, we calculated an effective collection efficiency of 1.5 percent, about an order of magnitude less than that found for systems using high numerical aperture microscope objectives as the relay optic [43]. In addition, the sampling efficiency would also be affected by the limited aperture of the relay optic as well as the beam size of the interrogating laser. The effective sampling efficiency in this system was determined to be 35 percent for fibers with numerical apertures of 0.14 and a core diameter of 8 μm. The mass detection limit (M_{dl}, moles) of the near-IR at a signal-to-noise ratio of 3 was determined by using the following expression:

$$M_{\mathrm{dl}} = \frac{3M_{\mathrm{inj}}(w_b B_{\mathrm{ave}})^{1/2}}{P_{\mathrm{area}}}$$

where M_{inj} is the mass injection volume (moles), w_b is the width of the peak in counting intervals, B^{ave} is the average background counting rate per time interval, and P_{area} is the area under the electrophoretic peak in counts. For the data shown in Fig. 8(B) at an applied field strength of 333 V/cm (M_{inj} = 10.0 attomoles, 1 attomole = 10^{-18} moles), the calculated mass detection limit was determined to be 2.8×10^{-19} moles. It would be anticipated that this mass detection limit could be significantly improved by the addition of organics into the running buffer, since these types of dye show improved fluorescence properties in organic solvents [43].

Conclusions

We have demonstrated the ability to produce micro-electrophoresis devices with high aspect ratios using X-ray lithography and a transfer or Kapton® mask. Due to the ability to micromachine with high aspect ratios, fine structures with three-dimensional shapes such as micro-optics and switching valves can easily be fabricated and integrated into the device. In addition, the use of the transfer or Kapton® mask methods allows one to investigate several different device configurations in order to optimize performance. These devices will be particularly attractive for DNA sample preparation and separation steps due to their low EOFs. Therefore, no wall coatings, which tend to break down when operated under high electric field conditions, are required. Therefore, this will significantly extend the operational lifetime of the device. Work is currently under way in our laboratory to demonstrate the utility of these devices for high-resolution separation of DNAs.

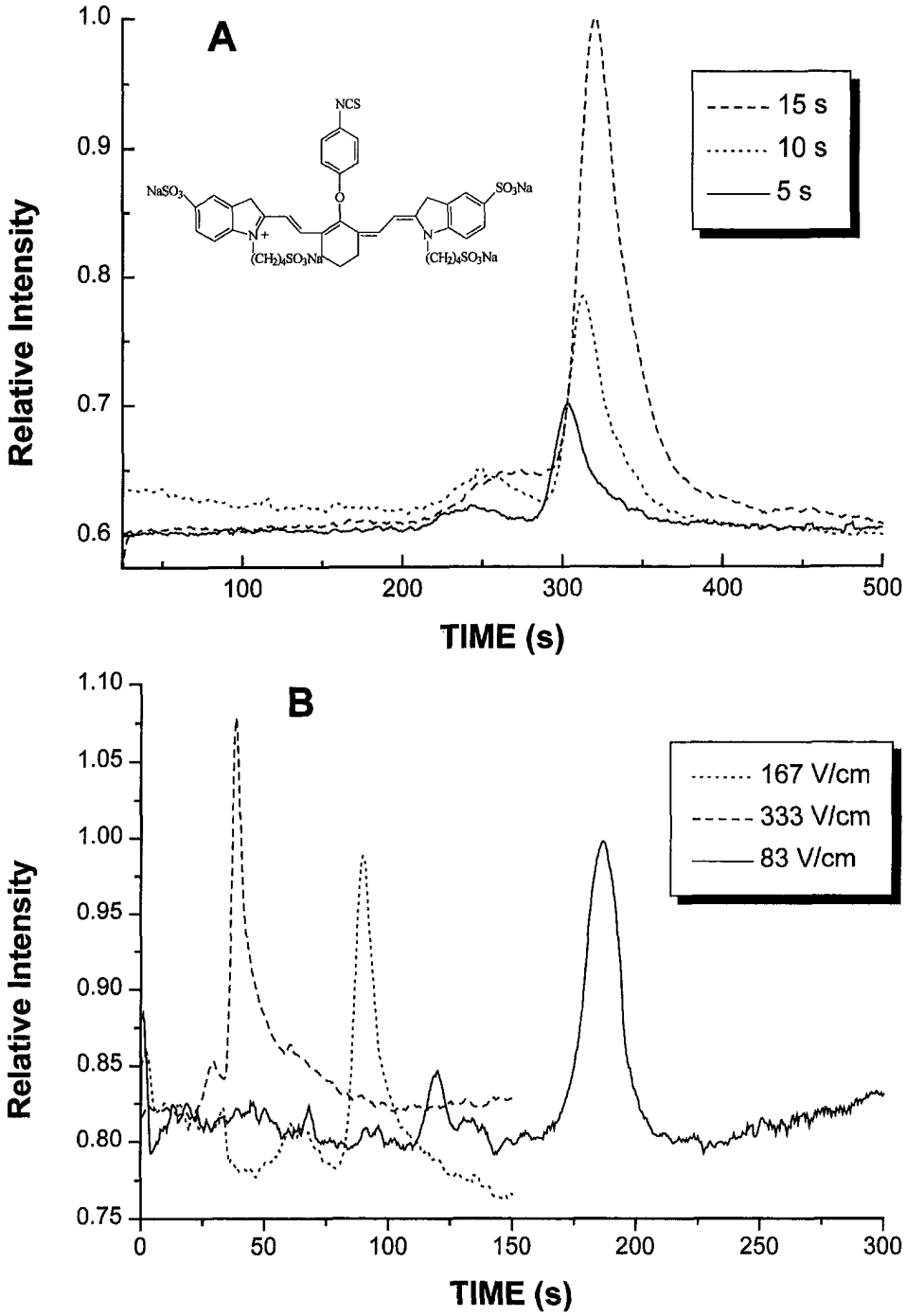

Fig. 8 Micro-electrophoresis of the near-IR dye, NN382 (see inset for chemical structure of dye), as a function of the injection time (A) and applied field strength (B). The run buffer in this set of experiments consisted of borate (20 mM, pH = 9.2). In all cases, the dye concentration used was 0.1 μM.

Acknowledgments

The authors would like to thank the Whitaker Foundation and the National Institutes of Health (R01 HG01499 and R29 HG00824) for financial support of this work. The authors would also like to thank CAMD for the use of the microfabrication facilities and the synchrotron beam line during the course of this work.

References

1 Heiger, D. N.; Cohen, A. S.; Karger, B. L., *J. Chromatogr.*, 1990, 516, 33–48.

2 Luckey, J. A.; Drossman, H.; Kostichka, A. J.; Mead, D. A.; D'Cuhna, J.; Swerdlow, H.; Gesteland, R., *Nucleic Acids Res.*, 1990, 18, 1415–1419.

3 Drossman, H.; Luckey, J. A.; Kostichka, A.; D'Cuhna, J.; Norris, T. B.; Smith, L. M., *Anal. Chem.*, 1990, 62, 900–903.

4 Chen, D.; Swerdlow, H. P.; Harke, H. R.; Zhang, J. Z.; Dovichi, N. J., *J. Chromatogr.*, 1991, 349, 812–813.

5 Schwartz, H. E.; Ulfelder, K.; Sunzeri, F. J.; Busch, M. P.; Brownlee, R. G., *J. Chromatogr.*, 1991, 559, 267–283.

6 Strege, M.; Lagu, A., *Anal. Chem.*, 1991, 63, 1233–1236.

7 Grossman, P. D.; Soane, D. S., *J. Chromatogr.*, 1991, 559, 257–266.

8 Pariat, Y. F.; Berka, J.; Heiger, D. N.; Schmitt, T.; Vilenchik, M.; Cohen, A. S.; Foret, F.; Karger, B. L., *J. Chromatogr.*, 1993, 652, 57–66.

9 Barron, A. E.; Soane, D. S.; Blanch, H. W., *J. Chromatogr.*, 1993, 652, 3–16.

10 Grossman, P. D., *J. Chromatogr.*, 1994, 663, 219–227.

11 Hjerten, S., *J. Chromatogr.,* 1985, 347, 191–198.
12 Grossman, P. D.; Colburn, J. C., *Capillary Electrophoresis: Theory and Practice,* Academic Press, 1992.
13 Harrison, J. D.; Fluri, K.; Seiler, K.; Fan, Z.; Effenhauser, C. S.; Manz, A., *Science,* 1993, 261, 895–897.
14 Effenhauser, C. S.; Manz, A.; Widmer, H. M., *Anal. Chem.,* 1993, 65, 2637–2642.
15 Fan, Z. H.; Harrison, J. D., *Anal. Chem.,* 1994, 66, 177–184.
16 Jacobson, S. C.; Hergenroder, R.; Koutny, L. B.; Warmack, R. J.; Ramsey, J. M., *Anal. Chem.,* 1994, 66, 1107–1113.
17 Jacobson, S. C.; Hergenroder, R.; Koutny, L. B.; Ramsey, J. M., *Anal. Chem.,* 1994, 66, 1114–1118.
18 Effenhauser, C. S.; Paulus, A.; Manz, A.; Widmer, H. M., *Anal. Chem.,* 1994, 66, 2949–2953.
19 Jacboson, S. C.; Koutny, L. B.; Hergenroder, R.; Moore, A. W.; Ramsey, J. M., *Anal. Chem.,* 1994, 66, 3472–3476.
20 Seiler, K.; Fan, Z. H.; Fluri, K.; Harrison, D. J., *Anal. Chem.,* 1994, 66, 3485–3491.
21 Jacobson, S. C.; Moore, A. W.; Ramsey, J. M., *Anal. Chem.,* 1995, 67, 2059–2063.
22 Effenhauser, C. S.; Manz, A.; Widmer, H. M., *Anal. Chem.,* 1995, 67, 2284–2287.
23 Woolley, A. T.; Mathies, R. A., *Anal. Chem.,* 1995, 67, 3676–3680.
24 Raymond, D. E.; Manz, A.; Widmer, H. M., *Anal. Chem.,* 1996, 68, 2515–2522.
25 Woolley, A. T.; Mathies, R. A., *Proc. Natl. Acad. Sci. U.S.A.,* 1994, 91, 11348–11352.
26 Jacobson, S. C.; Ramsey, J. M., *Anal. Chem.,* 1996, 68, 720–723.
27 Fluri, K.; Fitzpatrick, G.; Chiem, N.; Harrison, J. D., *Anal. Chem.,* 1996, 68, 4285–4290.
28 Fan, Z. H.; Harrison, J. D., *Anal. Chem.,* 1994, 66, 177–184.
29 Chiem, N.; Harrison, D. J., *Anal. Chem.,* 1997, 69, 373–378.
30 Woolley, A. T.; Hadley, D.; Landre, P.; DeMello, A. J.; Mathies, R. A.; Northrup, M. A., *Anal. Chem.,* 1996, 68, 4081–4086.
31 *Handbook of Microlithography, Micromachining and Microfabrication,* Vol. 1, P. Rai-Choudhury, ed., 1997.
32 Bley, P.; Goettert, J.; Harmening, M.; Himmelhaus, M.; Menz, W.; Mohr, J.; Muller, C.; Wallarabe, U., *Proc. Microsystem Technol.,* 1991, 302–314.
33 McCormick, R. M.; Nelson, R. J.; Alonso-Amigo, M. G.; Benvegnu, D. J.; Hooper, H. H., *Anal. Chem.,* 1997, 69, 2626–2630.
34 Effenhauser, C. S.; Bruin, G. J. M.; Paulus, A.; Ehrat, M., *Anal. Chem.,* 1997, 69, 3451–3457.
35 Martynova, L.; Locascio, L.; Galtan, M.; Kramer, G. W.; Christensen, R. G.; MacCrehan, W. A., *Anal. Chem.,* 1997, 69, 4783–4789.
36 Vladimirsky, Y.; Vladimirsky, O.; Saile, V.; Morris, K. J.; Klopf, J. M., *Proc. SPIE,* 1995, 2437, 391–395.
37 Vladimirsky, Y.; Vladimirsky, O.; Saile, V.; Morris, K. J.; Klopf, J. M., *Proc. SPIE,* 1995, 2621, 399–405.
38 Stadler, S.; Derhalli, I.; Malek, C. K., *SPIE Micromachining and Microfabrication,* 1997, 3225, 102–108.
39 Wollersheim, O.; Zumaque, H.; Mormes, J.; Kadereit, D.; Langen, J.; Häußling, L.; Hossel, P.; Hoffmann, G., *Nucl. Instrum. Methods B,* 1995, 1–6.
40 Ueno, N.; Kamiya, K.; Harada, Y.; Tinone, M.; Sekitani, T.; Tanaka, K., *Optoelectronics,* 1996, 11, 91–98.
41 Harrison, D. J.; Manz, A.; Fan, Z.; Lüdi, H.; Widmer, H. M., *Anal. Chem.,* 1992, 64, 1926–1932.
42 Flanagan, J. H.; Legendre, B. L.; Hammer, R. P.; Soper, S. A., *Anal. Chem.,* 1995, 67, 341–347.
43 Legendre, B. L.; Moberg, D. L.; Williams, D. C.; Soper, S. A., *J. Chromatogr.,* 1997, 779, 185–194.